Search efficiency of biased migration towards stationary or moving targets in heterogeneously structured environments

Youness Azimzade[1,2] and Alireza Mashaghi[2,*]
[1]*Department of Physics, University of Tehran, Tehran 14395-547, Iran*
[2]*Leiden Academic Centre for Drug Research, Faculty of Mathematics and Natural Sciences, Leiden University, Leiden 2300 RA, The Netherlands*
(Received 30 June 2017; revised manuscript received 30 October 2017; published 26 December 2017)

Efficient search acts as a strong selective force in biological systems ranging from cellular populations to predator-prey systems. The search processes commonly involve finding a stationary or mobile target within a heterogeneously structured environment where obstacles limit migration. An open generic question is whether random or directionally biased motions or a combination of both provide an optimal search efficiency and how that depends on the motility and density of targets and obstacles. To address this question, we develop a simple model that involves a random walker searching for its targets in a heterogeneous medium of bond percolation square lattice and used mean first passage time ($\langle T \rangle$) as an indication of average search time. Our analysis reveals a dual effect of directional bias on the minimum value of $\langle T \rangle$. For a homogeneous medium, directionality always decreases $\langle T \rangle$ and a pure directional migration (a ballistic motion) serves as the optimized strategy, while for a heterogeneous environment, we find that the optimized strategy involves a combination of directed and random migrations. The relative contribution of these modes is determined by the density of obstacles and motility of targets. Existence of randomness and motility of targets add to the efficiency of search. Our study reveals generic and simple rules that govern search efficiency. Our findings might find application in a number of areas including immunology, cell biology, ecology, and robotics.

DOI: 10.1103/PhysRevE.96.062415

I. INTRODUCTION

Migration and search are ubiquitous processes in biology [1] and generic principles may underlie these processes in seemingly distinct biological contexts. Many biological organisms and objects detect the spatial gradients of chemicals and respond to them by biased migration. Examples include mice navigation for odor sources [2], olfactory navigation in Drosophila [3], gradient sensing by amoebae and neutrophils [4], among others [5,6]. Biological cells and organisms may also show diffusive motions. During immune response, T cells need to detect cognate antigens at the surface of antigen-presenting cells and to interact with other immune cells. T cells accomplish these tasks through migration in lymphatic nodes or peripheral tissue [7]. T cell migration has been reported to be diffusive [8,9], subdiffusive [7,10], superdiffusive [11], or a combined migration [12]. However, it is not clear whether these different migration modes are internally controlled or are determined by environmental conditions [7].

How do target properties and the environment affect the search efficiency of a cell or organism? Search processes often happen in complex environments. In peripheral tissues, cells face heterogeneous extracellular matrix (ECM) and other cells [13] during their migration. ECM topography is able to guide cellular migration and regulate cellular motility through physical cues that geometrically constrain adhesion sites [14,15]. For example, T cells' velocity fluctuations have been attributed to morphology of lymphatic nodes [16] and the orientation of ECM fibrils affects direction of cellular migration [17–22]. From such examples, one can conclude that the physical structure of the environment is a determinant of search efficiency; yet, the dependency of the optimal mode of migration on the environmental heterogeneity is not fully understood. Further, we do not know how motility and density of targets affect the optimal search strategy. For example, the effect of motility of and frequency of antigen-presenting cells (APCs) as T cell targets on the T cell search efficiency has not been studied [7].

Here, we use simple models to look for generic rules that determine search efficiency in a heterogeneous environment and its dependency on density and motility of targets. Random motions in the absence or presence of obstacles have been studied widely in physics literature [23]. Presence of obstacles alters both the diffusion constant [24,25] and the dynamics of random motion [26–28] in a manner that depends on the density and structure of obstacles. Obstacles are expected to interfere with directionally biased motions because of creating dead end paths [29]; consequently, the mean velocity will be a nonmonotonic function of the bias and reaches zero for large biases at steady state [30,31]. For moderate times, similar behaviors were observed [32], but the extent of the interference has not been explored for short time periods and noncritical densities [33–40]. Here, we address this problem through simulation and quantify the efficiency using a key quantity that we borrow from studies on stochastic processes, namely, first passage time (FPT, T, also known as first hitting time) [41]. For an object searching for its target, FPT is a time that takes to reach the target for the first time. Mean first passage time (MFPT, $\langle T \rangle$) which quantifies the average time needed to reach a specific target, has been commonly considered as indicative of search efficiency [42–44]. MFPT has been calculated for both Markovian and non-Markovian walkers [45–49], but it has not been studied (neither analytically nor through simulation) for biased random walk in the absence or presence of obstacles. Furthermore, the effect of motility of targets (with both random and biased migration) and the effect of obstacles on this process has not been studied yet.

*Corresponding author: a.mashaghi.tabari@lacdr.leidenuniv.nl

As we explain in the following, our findings reveal generic rules that might be applicable to a wide range of problems including immune cell migration, where search efficiency is being intensely researched and MFTP has not yet been used as a measure of search efficiency [7,11].

II. MODEL

Random walk models have been successfully used to describe dynamics of a wide range of biological objects ranging from animal movement, dynamics of micro-organisms, to diffusion of biomolecules [50]. Generally, mean square displacement, $\langle r^2(t)\rangle$, for a randomly walking object can be written as

$$\langle r^2(t)\rangle = 4Dt^{\alpha} + \mathbf{v}^2 t^2 \tag{1}$$

in which D is the diffusion constant and $\mathbf{v}$ is the drift velocity, and if $\mathbf{v} = 0$ walk is simple random walk (SRW). In the presence of obstacles, diffusion constant changes from a fixed parameter to a location dependent parameter, yet the mean square displacement (MSD) and time remain linearly related (of course to a limited extent) as

$$\langle r^2(t)\rangle = 4D_{\text{eff}}t^{\alpha} \tag{2}$$

in which D_{eff} is the effective diffusion constant for the medium. As we will show in this paper, D_{eff} plays an essential role in the time scale of the events for simple random motion but not for directed motion. Without losing generality, we consider a two-dimensional (2D) lattice in which a walker is located at the center of a unit as its initial location and can jump to the centers of the nearest neighbor units. In this regard, jumping length would be equal to the distance between unit centers (or edge of each unit) δ at each time step (τ). In order to model environmental constraints, we consider each edge of these units as a potential obstacle. Thus, for each (x,y) point we define two parameters $E(x^+,y)$ and $E(x,y^+)$ for corresponding edges of each unit. When there is an obstacle ($E = 1$ or lines in Fig. 1) between two neighboring units, walker is not allowed to pass. Otherwise ($E = 0$, free space in Fig. 1), it is free to pass. As an initial condition, we screen all edges in the lattice and will consider each one as a solid line ($E = 1$) with probability of p and consequently no obstacle, $E = 0$, with probability of $1 - p$. (This process creates the square bond percolation model [51] for obstacles with occupancy equal to p and, respectively, the square bond percolation model for noncut paths with occupancy of $1 - p$; see Appendix)

Generally, the Fokker-Plank equation for this model would be as follows [50]:

$$\frac{\partial P(x,y,t)}{\partial t} = -\vec{\nabla}\cdot(\mathbf{v}P(x,y,t)) + \vec{\nabla}\cdot(\mathbf{D}\vec{\nabla}P(x,y,t)) \tag{3}$$

in which $\mathbf{v}(x,y) = \left[\begin{smallmatrix} b_1(x,y) \\ b_2(x,y)\end{smallmatrix}\right]$ and

$$\mathbf{D}(x,y) = \begin{bmatrix} a_{11}(x,y) & 0 \\ 0 & a_{22}(x,y)\end{bmatrix} = \begin{bmatrix} D_x(x,y) & 0 \\ 0 & D_y(x,y)\end{bmatrix}$$

with $b_1 = \delta[r(x,y) - l(x,y)]/\tau$, $b_2 = \delta[u(x,y) - d(x,y)]/\tau$, $a_{11}(x,y) = \delta^2[r(x,y) + l(x,y)]/2\tau$, $a_{22}(x,y) = \delta^2[u(x,y) + d(x,y)]/2\tau$ where $r(x,y)$, $l(x,y)$, $u(x,y)$, and $d(x,y)$ are the probabilities of going right, left, up and the down for a single walker and for a SRW we have $r = l = u = d = \frac{1}{4}$ (for more details, see Appendix).

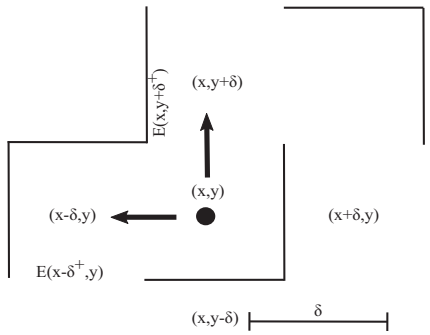

FIG. 1. Illustration of a searching walker within a structured medium. The walker cannot jump to the neighboring units separated by a solid line (corresponding E is equal to one), while it is free to jump otherwise (corresponding E is equal to zero). As such, in this figure, the walker at (x,y) is only allowed to move in depicted directions. As an initial condition, each line will be considered solid with probability of p. (This process creates the square bond percolation model for obstacles with occupation equal to p and, respectively, the square bond percolation model for for noncut paths with probability of $1 - p$; see Appendix.)

III. RESULTS

To study the effect of environmental obstacles (which in our model are solid lines and their number is proportional to the value of p) on migration of walkers, we simulate the motion of 10^5 walkers separately moving on bond percolation lattice based on Eq. (3) with $\mathbf{v} = 0$. For $\mathbf{v} = 0$ and different values of p we calculated the mean square displacement [MSD or $\langle r^2(t)\rangle$] by averaging over trajectories of all independent walkers in a 600×600 lattice and for 600 time steps (probability of reaching to the border of lattice in 600 steps is quite small and we could be sure that none of the searching walkers would reach the border).

We first focus on search efficiency of simple random walkers. We can readily extract the main macroscopic feature of simple random walk, i.e., diffusion constant D, through analysis of $\langle r^2(t)\rangle$. When p increases, searching walkers will migrate slower, but we define an effective diffusion constant D_{eff} as the indication of average diffusion constant for the whole medium [see Fig. 2(a)]. Using variation of MSD per time and $\langle r^2(t)\rangle = 4D_{\text{eff}}t$, we calculate the value of D_{eff} for different values of p [Fig. 2(b)]. To analyze the search efficiency of random walkers, we need to calculate FPT (T) and its average MFPT ($\langle T\rangle$). To do so, we simulate the random walk process on relative percolation lattice for 10^5 independent walkers and find the time T that it takes for every searching walker to reach the target. To be consistent with previous studies and to create comparable results, we work with normalized MFPT, $\langle T\rangle/N$, in which N is the number of sites which the walker can visit (for distribution of T, see Appendix). In agreement with previous results [52], the value of $\langle T\rangle D_{\text{eff}}/N$ fits nicely the universal curve of $\ln(R)$ in which R is the distance between initial place of searching walkers and their target [Fig. 2(c)].

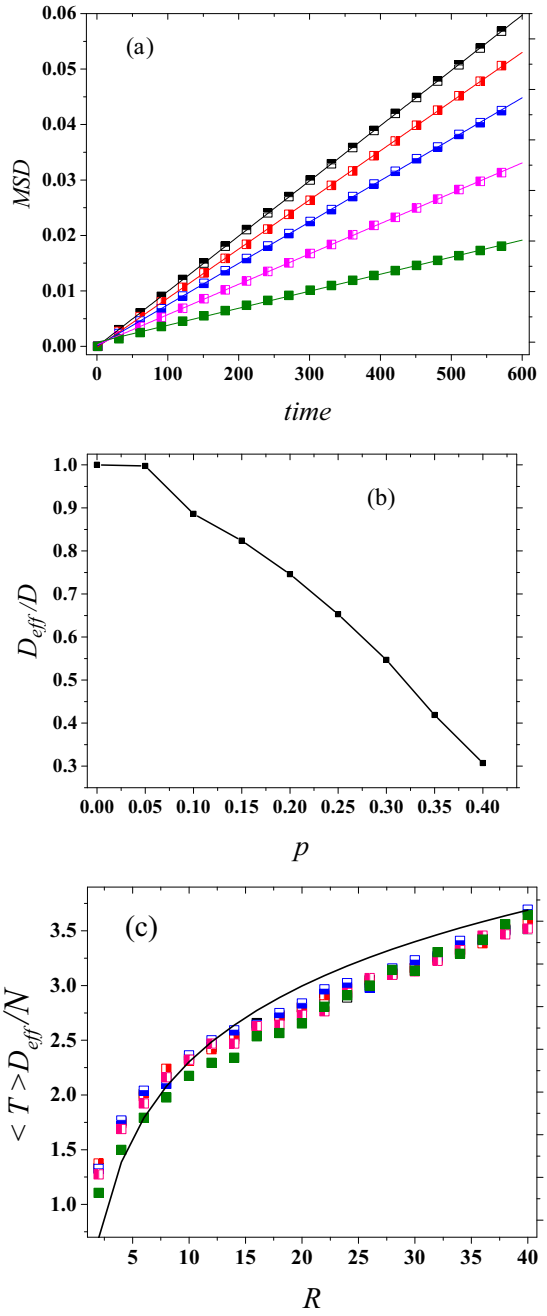

FIG. 2. (a) Evolution of MSD per time for different values of p ($p = 0$, 0.1, 0.2, 0.3, and 0.4 from top to bottom) in units of jumping length δ and time step τ. Linear behavior, which remains for $p < p_c = 0.5$, indicates diffusionlike motion for walkers and the slopes of fitted lines are equal to $4D_{\text{eff}}$ for each p. (b) D_{eff}/D versus p. (c) Normalized MFPT, $\langle T\rangle D_{\text{eff}}/N$, per distances between the initial place of walkers and their target R for different values of p fits to the universal diagram of $\ln(R)$ (the solid line). In agreement with previous results [52], this figure shows that D_{eff} regulates the time scale of search. SEMs for all cases are smaller than symbol size.

Next, we study directionally biased migration in the presence of obstacles. We consider that a walker that starts searching from its initial location (x_0, y_0) tends to migrate toward a target at (x', y'). Biological entities can detect the local gradients of chemicals and respond to them by moving toward the source of chemicals [2–6]. Based on the Keller-Segel model [53], this process can be modeled through choosing the direction towards the target with a higher probability (see Appendix). In such a case, the probability of moving in the right direction at any (x, y) position can be defined as below (other probabilities also change the same) *which can be higher or lower than other probabilities based on the the values of* x *and* x':

$$r(x,y) = \frac{1 - E(x^+, y)}{S(x,y)} \frac{e^{\gamma|x-x'|}}{e^{\gamma|x-\delta-x'|}} \tag{4}$$

in which γ is the strength of migration towards the target *and is formed of ability of entities to detect and respond to chemical gradient*. $\gamma = 0$ indicates SRW (for l, δ changes to $-\delta$ and for u and d, y takes the place of x) and $S(x, y)$ is again the normalization factor which ensures $r + l + u + d = 1$. For $p = 0$, we have $b_1 = \pm b_2 = \mp\delta(e^{\gamma\delta} - e^{-\gamma\delta})/\tau S(x, y)$ and $a_{11}(x, y) = a_{22}(x, y) = \delta^2(e^{\gamma\delta} + e^{-\gamma\delta})/\tau S(x, y)$. When γ approaches 3.5, migration changes to an entirely directed (ballistic) motion towards the target [Fig. 3(a)]. To understand the effect of directionality of migration on search efficiency, we analyzed $\langle T\rangle$ per R for different values of directionality γ. When we increase the directionality of motion, behavior of $\langle T\rangle/N$ per R changes from $\ln(R)$ for SRW to R/v for ballistic motion in which v is the migration velocity.

As Fig. 3(b) indicates, for $p = 0$ and a fixed value of R, MFPT is a univocally decreasing function of γ which means that directionality of motion always increases the search efficiency and for $\gamma > 3$ $\langle T\rangle/N$ reaches to its minimum $\langle T\rangle^*/N$, which is the time needed for directly moving from initial place towards target divided by the factor N. While for a nonzero p, the behavior of $\langle T\rangle/N$ per γ is not univocal [Fig. 3(b)]. For each nonzero value of p, there is a γ^* that creates the minimum value of $\langle T\rangle/N$ which identifies the optimized search strategy. This result implies that in a heterogeneous medium, a purely random or purely directed migration towards target is not the optimized strategy. Instead, a combination of directed and random motion is the optimal choice and the density of obstacles determines the contributions of each mode.

Next, we ask how target frequencies and motility of targets affect search efficiency. Number of randomly distributed targets within medium n regulates the value of $\langle T\rangle/N$ through decreasing the distance in which we expect the searching walker to see a target by the factor of $\sqrt{n}$ and, consequently, $\langle T\rangle/N$ with the factor of n. Furthermore, instead of a fixed target, we consider that at each time step, the target is able to move randomly by probability of p_m or remains at its location with probability of $1 - p_m$. In the targets' frame of reference, target is fixed but at each time step the walker moves $1 + p_m$ times. As a result, after M steps it had moved $M \times (1 + p_m)$ times and $\langle T\rangle/N$ should decrease by the factor of $(1 + p_m)$.

As another possibility, we considered a walker chasing a target which in turn moves randomly. Effects of directionality of motion and density of obstacles were studied [Fig. 4(a)]. Finally, it may happen that both targets and walkers search for each other according to Eq. (4) [Fig. 4(b)]. Migration of target (both randomly and towards searching walkers) does not

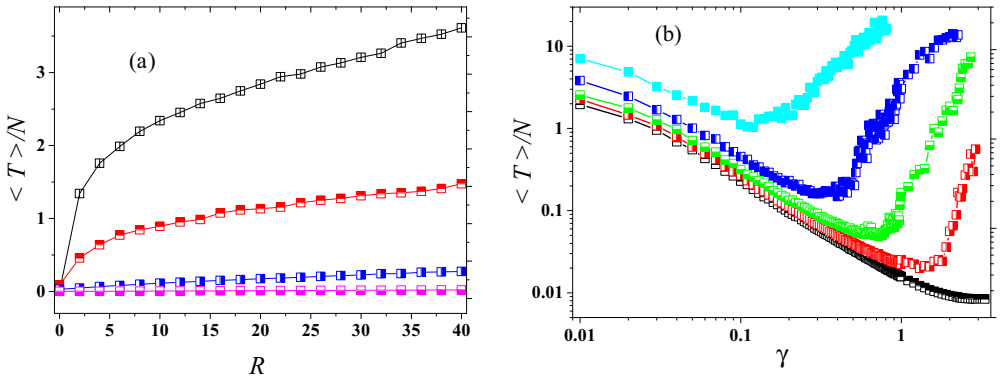

FIG. 3. (a) Variation of $\langle T\rangle/N$ per R for $p = 0$ and $\gamma = 0, 0.02, 0.1$, and 1 from top to bottom. As γ increases, $\langle T\rangle/N$ changes from $ln(R)$ for a random walker to R/v for ballistic motion in which v is the migration velocity. (b) Changes of $\langle T\rangle/N$ per γ for $R = 30$ and $p = 0.4$, 0.3, 0.2, 0.1, and 0.0 from top to bottom. As p increases, $\langle T\rangle/N$ deviates from the univocal behavior. For larger values of p, there is a γ^* at which walkers have the minimum value for $\langle T\rangle$. For $p = 0.4$, $p = 0.3$, $p = 0.2$ and $p = 0.1$, $\gamma^* = 0.12$, $\gamma^* = 0.4$, $\gamma^* = 0.72$ and $\gamma^* = 1.3$, respectively, are creating $\langle T\rangle^*/N$. Standard error of the means (SEMs) for all cases are smaller than symbol size.

change the general behavior of $\langle T\rangle/N$ for different values of p but the value of γ for corresponding optimized search strategy γ^* would be different [Fig. 4(c)]. Dynamics of $\langle T\rangle^*/N$ for all studied cases was obtained [Fig. 4(d)].

Using MSD analysis to study random walk is not reliable for all cases [54,55]. For small values of γ, MSD does not change whereas $\langle T\rangle$ might change dramatically. Besides, for larger values of γ when we increase the value of p, analysis of MSD shows that a superdiffusive motion is gradually converted to a diffusive motion and then to a subdiffusive motion.

The results of our study can be generically applied to a wide range of problems including cell migration, animal movements, and dynamics of nonbiological microparticles. For example, as shown in the Appendix, our findings can be applied to shed light on some of current open problems related to T cell migration.

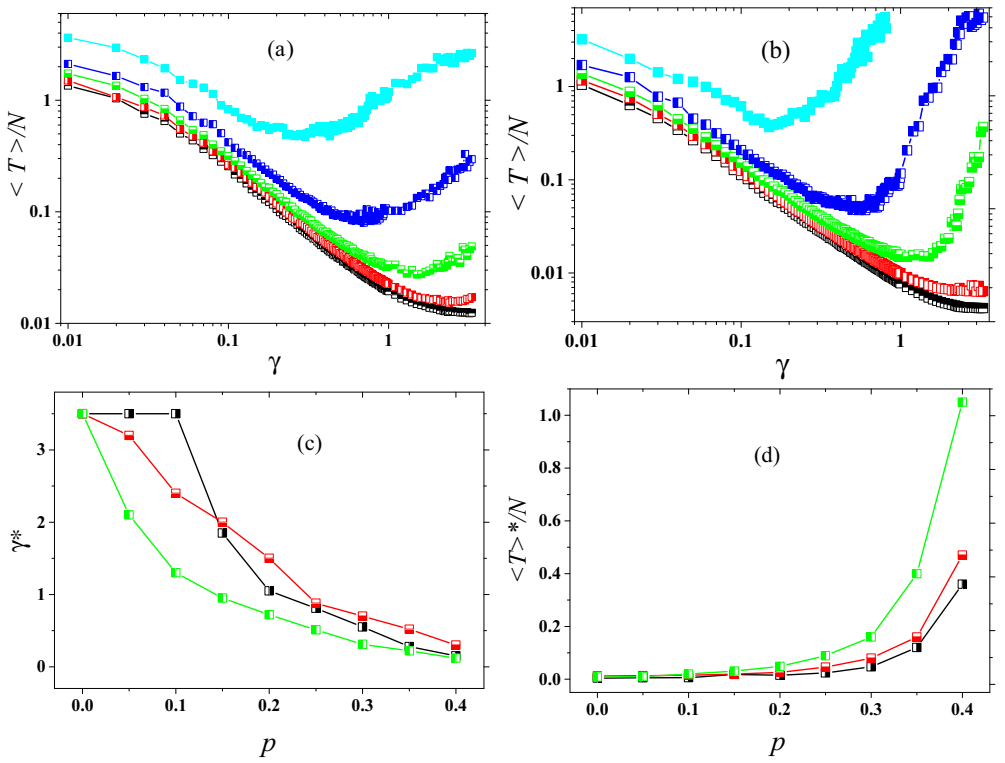

FIG. 4. (a) Behavior of $\langle T\rangle/N$ per γ when walker migrates towards the target with directionality of γ and the target itself moves randomly for $p = 0.4$, 0.3, 0.2, 0.1, and 0.0 from top to bottom. (b) Behavior of $\langle T\rangle/N$ per γ when both target and walker migrate towards each other with directionality of γ for $p = 0.4$, 0.3, 0.2, 0.1, and 0.0 from top to bottom. (c) Behavior of γ^* as the γ which minimizes $\langle T\rangle/N$ and consequently generates the optimized search strategy for biased migration (half-right square), random migration (half-down square), and fixed targets (half-left square). (d) Behavior of $\langle T\rangle^*/N$ as the minimum value of $\langle T\rangle/N$ for biased migration (half-right square), random migration (half-down square), and fixed targets (half-left square). SEMs for all cases are smaller than symbol size (see Appendix).

IV. DISCUSSION

Here, we simulated a wide range of migration dynamics from random migration to a pure directed migration towards targets and studied the unexplored effect of directional bias on $\langle T \rangle$ and density of obstacles and motility of targets. Expectedly, we find that density of obstacles does not change the $\langle T \rangle$ for simple random walk. For a directionally biased migration, directionality always decreases $\langle T \rangle$ in the absence of obstacle, and the minimum value of $\langle T \rangle$ as the indication of the optimized migration strategy corresponds to the largest directionality $\gamma^* \sim 3.5$ (ballistic motion). In the presence of obstacles, instead of a pure directed motion, a combined motion, $0 < \gamma^* < 3.5$, leads to the minimum value of $\langle T \rangle$ and thus the optimized search strategy. The physical structure of environment thus dramatically affects search efficiency, and randomness plays a beneficial role in finding targets. When the target frequency increases or the targets are able to migrate (both randomly and directed towards walker), they are easier to find (not for higher values of p). In the presence of obstacles, directionality plays the same dual role. Finally, physical obstacles could change the dynamics of motion and convert a superdiffusive motion to a subdiffusive one.

ACKNOWLEDGMENTS

We acknowledge A. Gerard and M. Javadi for reading our manuscript and their comments. We also thank Department of Physics, Tehran University, for the computational facility.

APPENDIX

1. Bond percolation model on square lattice

The model we use to describe the obstacles is analogous to bond percolation model on square lattice [51] with occupancy equal to p; but, instead of bonds, we are working with lattice units which are confined with these bonds. Besides, paths walker could migrate through belong to a bond percolation square lattice with occupancy equal to $1 - p$ (Fig. 5).

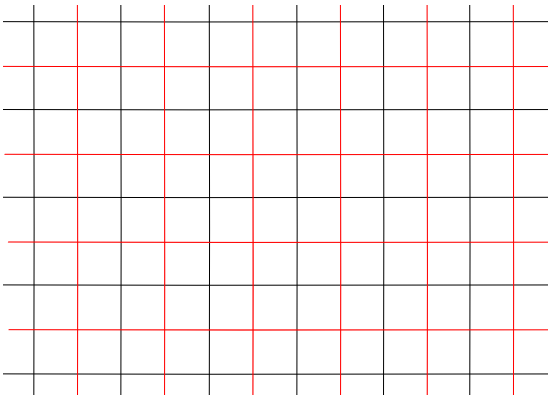

FIG. 5. Black (dark gray) edges are the boundary of units and red (light gray) edges connect the center of units. When we consider existence of black edges with probability of p, the crossing red edges would be cut by probability of p and will remain with probability of $1 - p$. As a result, red edges together generate a square bond percolation with occupancy equal to $1 - p$.

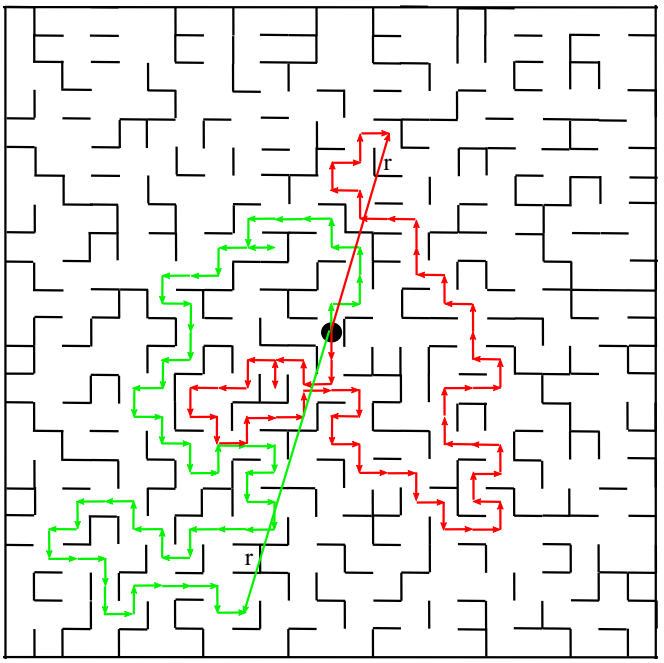

FIG. 6. Motion of two walkers at medium with $p = 0.4$.

2. Simulation process of migration in heterogeneous media

For a given initial configuration of the environment, probabilities of jumping at different directions are given by $l(x,y) = \frac{1-E(x^+,y)}{S(x,y)}$, $r(x,y) = \frac{1-E(x+\delta^+,y)}{S(x,y)}$, $u(x,y) = \frac{1-E(x,y+\delta^+)}{S(x,y)}$, and $d(x,y) = \frac{1-E(x,y^+)}{S(x,y)}$, where $S(x,y)$ is the normalization factor for these probabilities and we have $S(x,y) = 4 - E(x^+,y) - E(x+\delta^+) - E(x,y^+) - E(x,y+\delta^+)$. During simulation, each walker moves based on the the given probabilities which are under effect of position of obstacles. Diffusion of walkers on lattice would be regulated by barriers. To deeply understand the effect of barriers, consider the corresponding Langevin equation as the equation of motion of walkers. Remind that this Langevin equation is the continuum limit of the random walk and if we discrete the space and time, the Langevin equation would be the description of random walk on lattice. For simple random walker (SRW) we have $b_1 = b_2 = 0$ and for SRW with $p = 0$, $a_{11} = a_{22} = D_x = D_y = D/\sqrt{2}$. For other values of p, a_{11} and a_{22} (consequently D_x and D_y) would be determined locally based on the presence of obstacles. Each walker during migration calculates these probabilities and moves based on them (Fig. 6). Langevin equation of $\frac{\partial P(x,y,t)}{\partial t} = -\vec{\nabla} \cdot (\mathbf{v}P(x,y,t)) + \vec{\nabla} \cdot (\mathbf{D}\vec{\nabla}P(x,y,t))$ is $\dot{r} = \mathbf{v} + \sqrt{D}\eta(r,t)$ with $\langle \eta(r',t')\eta(r,t) \rangle = \delta_{t,t'}\delta_{r,r'}$.

3. Speed fluctuation

As shown in Figs. 7 and 8, location of the walker and its velocity significantly fluctuate in time. As Figs. 7–9 show, a quite random motion could have different phases. A reliable analysis of searching walker dynamics should consider longer time scales and large number of searching walker in order to obtain accurate results.

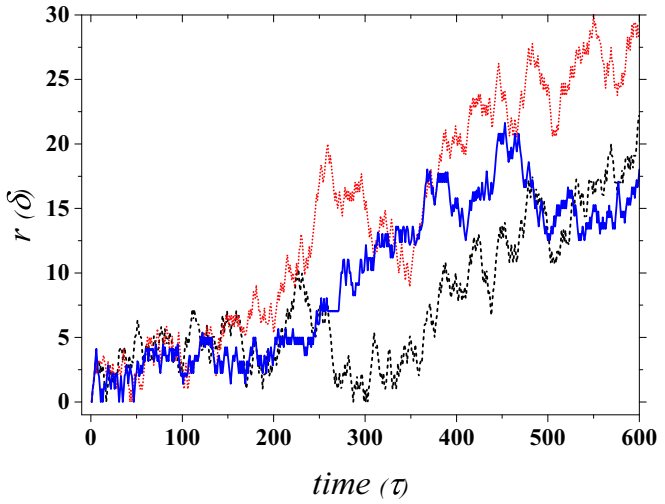

FIG. 7. Position of three walkers at different media as a function of time for $p = 0$ as the short dashed line, $p = 0.2$ as the short dotted line, and $p = 0.4$ as the solid line.

4. Informed random walk and chemotaxis

Different animals have been shown to recognize and orient towards odors over distances from a few hundred meters to few tens of kilometers [56]. Chemotactic cues are able to navigate cells up to few millimeters [57–59]. For a single chemoattractant secreting cell, the chemotactic response can be seen for ∼200 μm [58] distances. One very common model for chemotaxis is the Keller-Segel model [53] in which for cells centered at x, the probability of steps to the right and left will be given by $F[c(x+\delta)-c(x)]$ and $F[c(x-\delta)-c(x)]$. δ is the migration length, $c(x)$ is the concentration of chemoattractant at x, and F is an increasing function. By considering $c(x) \propto 1/|x-x'|$ in which x' is the location of source on x axis and $F(c) \propto e^{(\gamma c)}$ for the probability of steps to the right r, we have $r \propto \frac{e^{\gamma|x-x'|}}{e^{\gamma|x-\delta-x'|}}$ and for the probability of steps to the left l, we have $l \propto \frac{e^{\gamma|x-x'|}}{e^{\gamma|x+\delta-x'|}}$. Expanding model to 2D and adding the presence of obstacles reads as

$$r(x,y) = \frac{1-E(x^+,y)}{S(x,y)} \frac{e^{\gamma|x-x'|}}{e^{\gamma|x-\delta-x'|}},$$

$$l(x,y) = \frac{1-E(x^+,y)}{S(x,y)} \frac{e^{\gamma|x-x'|}}{e^{\gamma|x+\delta-x'|}}.$$

For the case of fixed target, the mentioned approach distribution of chemoattractant works properly. The effect of motility of targets on chemoattractant distribution needs more clarification. Chemoattractants diffusion constant has been reported to be $D_{\text{chem}} \sim 7\times10^{-7}$ cm^2/s [60]. Based on $\langle r^2(t)\rangle = 4D_{\text{chem}}t$ and $r \sim 300$ μm, chemoattractants travel the longest distance in our model in few minutes. Since this time is smaller than our model time step, 10 min, our approach for simultaneously updating distribution of chemoattractants remains valid.

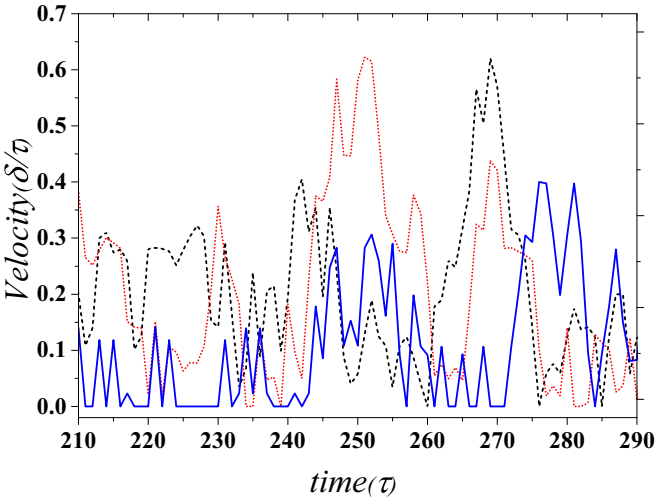

FIG. 8. Average velocity of the same walkers for 10 time steps for $p = 0$ as the short dashed line, $p = 0.2$ as the short dotted line, and $p = 0.4$ as the solid line. Speed fluctuations for different values of p can been seen. Speed fluctuations appear at short time scales, and might be interpreted as different migration dynamics.

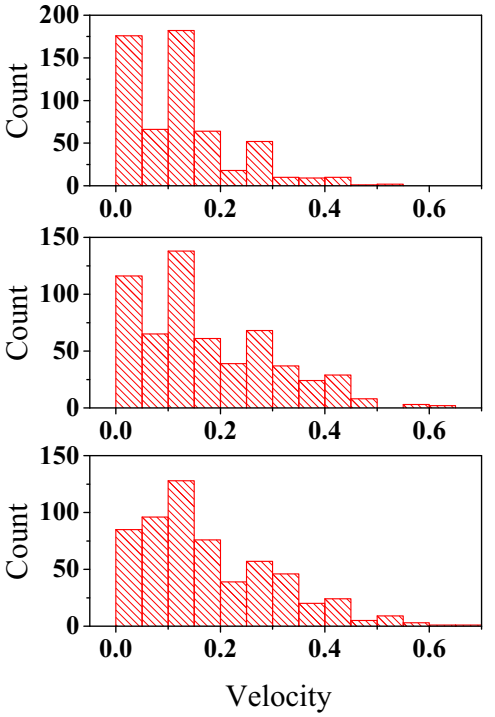

FIG. 9. Histogram of average velocities for 10 time steps for $p = 0.4$, 0.2, and 0.0 from top to bottom. which is in qualitative agreement with reports for T cells [8] with $\delta = 10$ μm and $\tau = 1$ min.

5. Spatial distribution of walkers

Probability density function (PDF) of x (y) which represents the probability of finding the walker at position x (y) at t obeys

$$\phi(x,t) = \frac{1}{\sqrt{4\pi D_x t}} e^{\frac{-x^2}{4D_x t}},$$

$$\phi(y,t) = \frac{1}{\sqrt{4\pi D_y t}} e^{\frac{-y^2}{4D_y t}}.$$

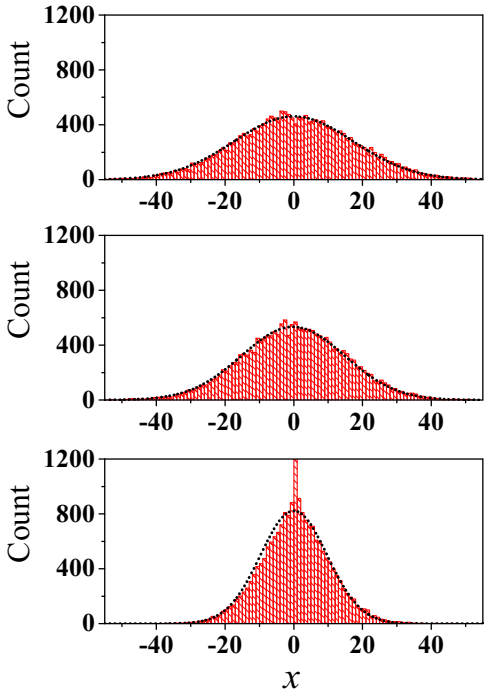

FIG. 10. Distribution of x which deviates from normal distribution for large values of p for $p = 0$, 0.2, and 0.4 from top to bottom. For larger values of p, the distribution starts to deviate from normal distribution but the best fitted normal distribution curves' standard deviation is governed by $\sqrt{D_{\text{eff}}}$.

But, for larger values of p, distributions of x and y start to deviate from normal distribution (Fig. 10). These new distributions are governed by $\sqrt{D_{\text{eff}}}$ but MSD still shows linear dependency on time (Fig. 2). Within a heterogeneous medium with fractal structures, dynamics of the motion has been demonstrated to be related to fractal dimension and spectral dimension of the structures [26–28]. For other distributions of physical obstacles, it has been shown that dynamics of motion and diffusion constant are related to density of obstacles. Randomly distributed fixed obstacles can decrease diffusion constant [24,25].

6. MSD analysis

During our analysis we considered MSD diagram versus time as our reference to analyze migration dynamics of walkers and obtain D_{eff}. However, log/log diagram of MSD versus time shows the dynamics of motion with higher accuracy (Fig. 11). As Fig. 11 shows, for $p = 0.4$ the dynamics of migration changes to subdiffusive but our calculations based on D_{eff} remain valid most probably because of negligible effect of this variation as seen in Fig. 2. Besides, even if we eliminate the case of $p = 0.4$ because of appearance of subdiffusive behavior, our main results remain valid for smaller values of p in which $p \sim 1$.

Using MSD analysis to study random walk is not reliable for all cases [54,55]. For small values of $\gamma = 0.005$, MSD does not change whereas $\langle T \rangle$ decreases by 25%. Besides, for larger values of γ, i.e., $\gamma = 0.07$, when we increase the value of p, analysis of MSD shows that a superdiffusive motion

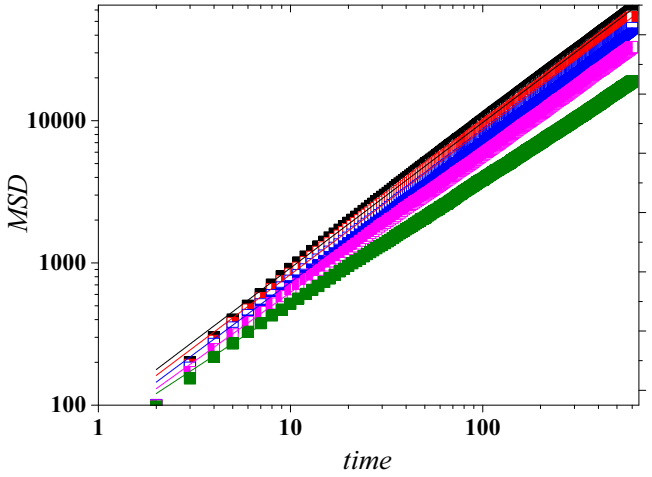

FIG. 11. MSD versus time in log/log diagram for $p = 0$ with $\alpha = 1.02$, $p = 0.1$ with $\alpha = 1.02$, $p = 2$ with $\alpha = 1.0$, $p = 0.3$ with $\alpha = 0.97$, and $p = 0.4$ with $\alpha = 0.87$ from top to bottom. For $p = 0.4$, α deviates from 1 but the general analogy we used still works properly. For each case, error in the value of α is less than 0.02.

($\alpha = 1.15$) gradually is converted to a diffusive ($\alpha = 1.0$) motion and then to a subdiffusive motion ($\alpha = 0.85$) (Fig. 12).

7. Distribution of T

By now we have studied the behavior of MFPT. Here, we aim to study FPT itself and its distribution. Distribution of T is not like normal distribution. Instead, it has skewness which seems to be log-normal distribution [61] which changes by time and variations in γ and p. Random variable x is

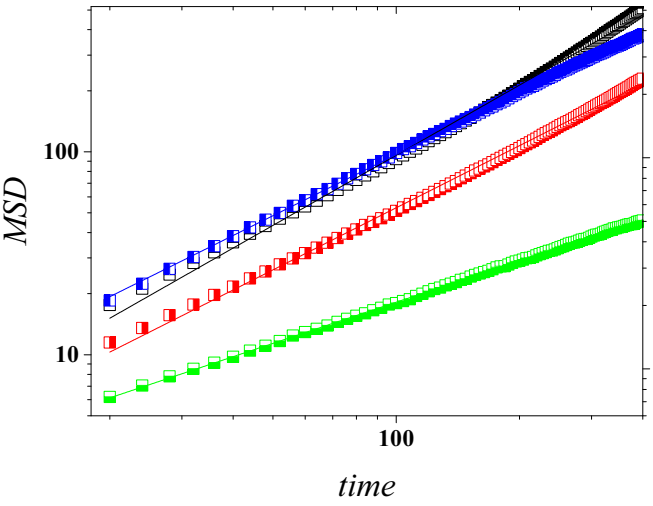

FIG. 12. MSD for different values of p and γ at δ units $\gamma = 0.07$, $p = 0$, and $\alpha = 1.15$ (black half-up square); $\gamma = 0.07$, $p = 0.3$, and $\alpha = 1.02$ (red half-right square); $\gamma = 0.07$, $p = 0.42$, and $\alpha = 0.85$ (green half-down square); $\gamma = 0.005$, $p = 0$, and $\alpha = 1.00$ (blue half-left square). As this figure indicates, for $\gamma = 0.07$ the value of α changes from 1.15 ± 0.01 to 0.85 ± 0.01 for different values of p. This variation indicates the fact that physical obstacles are capable of altering the whole dynamics of motion. Also, for $\gamma = 0.005$ in which the value of $\langle T \rangle$ decreases 30%, we still have $\alpha = 1.002 \pm 0.001$.

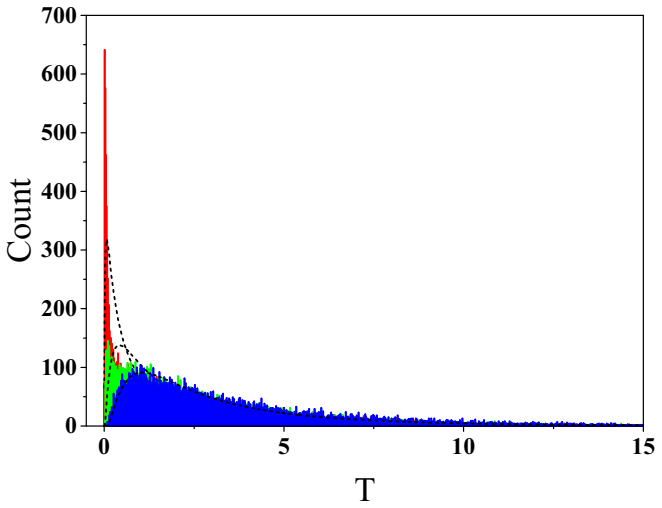

FIG. 13. Distribution of FPT, T, for $R = 10$ (red), $R = 20$ (green), and $R = 40$ (blue)with $\gamma = p = 0$.

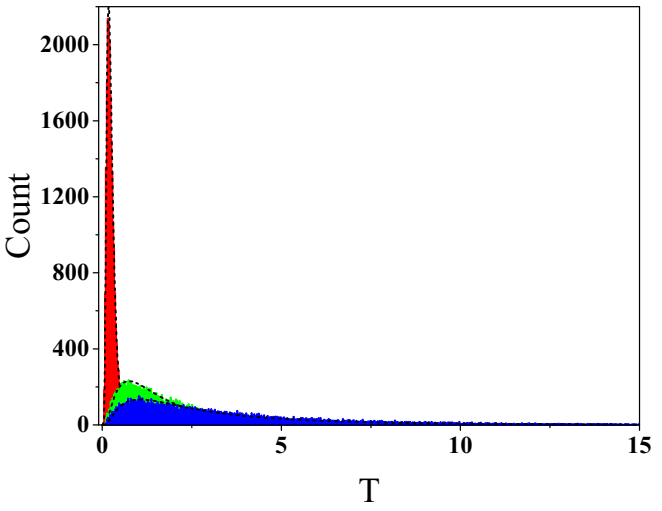

FIG. 15. Distribution of FPT, T, for $\gamma = 0.1$ (red), $\gamma = 0.01$ (green), and $\gamma = 0$ (blue) with $p = 0$ and $R = 40$.

log-normally distributed if $\log(x)$ has a normal distribution. For a qualitative comparison, in each case we have shown the fitted log-normal curves. Also, distribution of $\log(T)$ would be an appropriate candidate to see how much the distribution of T is comparable to log-normal distribution. Analogous to $\langle T \rangle$, T tends to increase for larger values of p and decrease for larger values of γ. But, it also exhibits variations in distribution (Figs. 13–15).

8. Visualizing search efficiency

When we have $p = 0$, a directed migration towards target is the most efficient strategy to reach target. As we move from directed migration toward random migration, the efficiency will decrease. Figures 16(a) and 16(b) show that for a free space, a directed migration with $\gamma = 0.5$ reaches to the target when the other walker with $\gamma = 0.125$ has passed less than half of its way towards the target. Contrary to what happens for free space, in the crowded space with a lots of obstacles, the walker with lower directionality is able to reach the target in a shorter time with respect to the walker with higher directionality [Figs. 16(c) and 16(d)].

A closer look at migration in the medium with obstacles will provide deeper understanding. Figure 17 shows migration with different directionality at a crowded medium. For $\gamma = 0.5$, the walker will choose the direction towards the target with probability of seven times larger than $\gamma = 0.125$. This high directionality leads to a smaller number of choices for these walkers. As a result, when there is no straight way towards target, these walkers will face troubles in finding their way. They usually choose the direction which minimizes their distance with target. Double sided vectors indicate the edges that the walker might be trapped in. At each side of these edges, the walker finds the other side as a point with higher probability. When γ approaches 1, the walker could be trapped

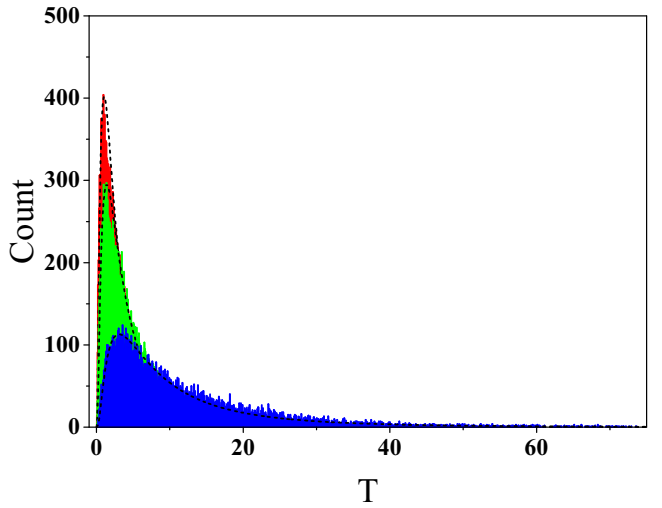

FIG. 14. Distribution of FPT, T, for $p = 0$ (red), $p = 0.2$ (green), and $p = 0.4$ (blue) with $R = 40$ and $\gamma = 0$.

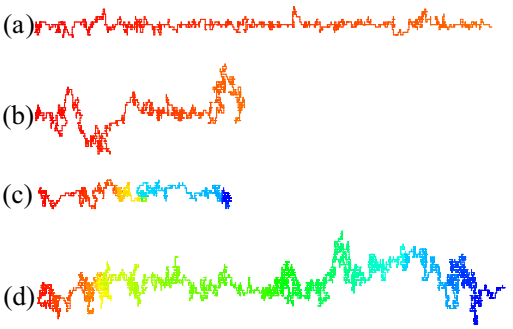

FIG. 16. Migration of two walkers with directionalities of $\gamma = 0.125$ and 0.5 for $p = 0$ and 0.4. For free space, $p = 0$, the directed migration (a) will arrive in a shorter time. While the walker with lower directionality (b) has passed half of its way towards the target. When the density of obstacles increases at medium, the walker with higher directionality moves slower than the other walker. For $p = 0.4$ (c), the walker just passed the half of distance between the initial place and the target when the other walker (d) has reached the target (colors have the same scale and they indicate time).

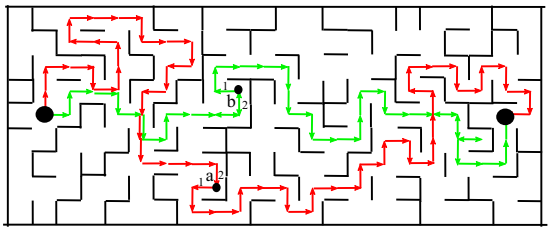

FIG. 17. Migration with different directionalities, red vectors with $\gamma = 0.125$, and green vectors with $\gamma = 0.5$. At points a and b, probability of taking direction of 1 at point b is about half of the probability of taking the direction of 1 at point a whereas these two points are identical.

in any set of these edges for unlimited times. On the other hand, the walker with $\gamma = 0.125$ chooses its direction rather freely and the chance of being trapped is much lower for this walker. For point a in Fig. 17, the probability of going the direction of 1 is equal to

$$\frac{e^{-\gamma\delta}}{e^{-\gamma\delta} + e^{\gamma\delta}} = 0.4$$

with $\gamma = 0.125$ while at point b the probability of going the direction of 1 is equal to

$$\frac{e^{-\gamma\delta}}{e^{-\gamma\delta} + e^{\gamma\delta}} = 0.27$$

with $\gamma = 0.5$. As a result, the walker with $\gamma = 0.125$ can escape such positions faster than the walker with $\gamma = 0.5$. Note that these probabilities should be multiplied to get the final probability of escape and, consequently, this difference will be multiplied.

9. Medium size effect

Size of medium which walkers are moving in it has been shown to have no effect on $\langle T\rangle/N$ in which N is the number of sites which walker can visit. In this regard, we calculated

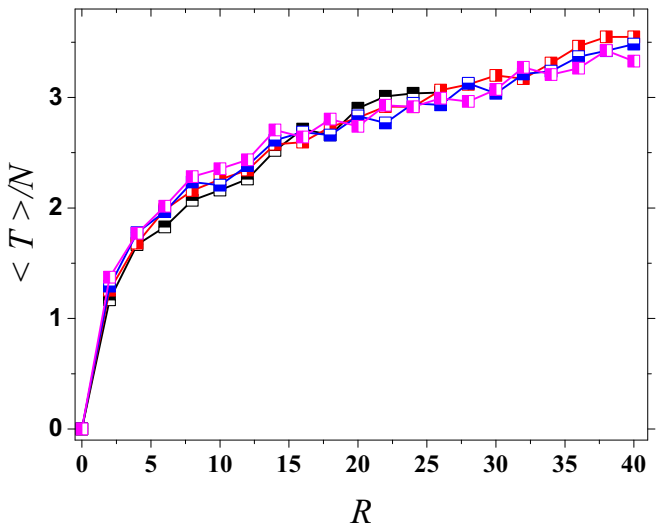

FIG. 18. Effect of size of lattice on $\langle T\rangle/N$ per R in δ units ($\delta = 10\ \mu$m) with $N = L \times L$ for $L = 30$ (black), $L = 50$ (red), $L = 70$ (blue), and $L = 100$ (magenta).

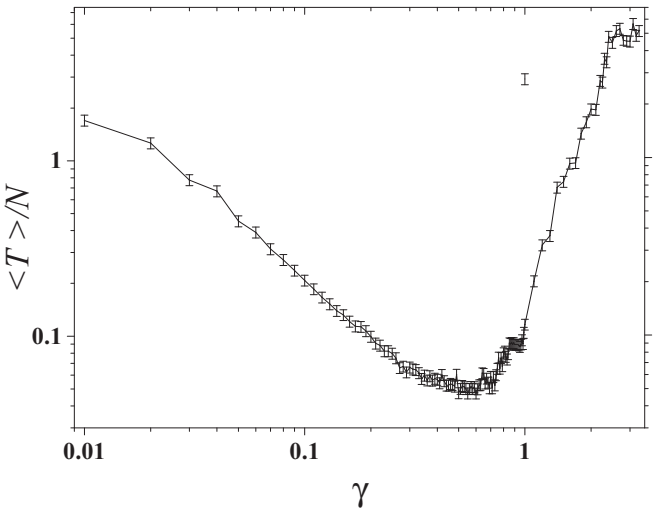

FIG. 19. Standard error of mean of MFPT, $\langle T\rangle/N$, versus γ with $p = 0.4$ and $R = 40$.

$\langle T\rangle/N$ for lattice with different sizes and Fig. 18 shows that it does not depend on lattice size.

10. Error analysis

In all graphs, the value of standard error of mean has been smaller than the size of symbol. Here is the SEM for some cases (Fig. 19).

11. Effect of number and motility of targets

When the motility of target increases (except for small values of p_m when $p = 0$ in which $\langle T\rangle/N$ starts to increase), $\langle T\rangle/N$ decreases. This result is understandable through relative reference frame. In the targets' frame of reference, the target is fixed but at each time step the walker moves $1 + p_m$ times. As a result, after M steps we have $\langle r^2\rangle = M(1 + p_m)D_{\text{eff}}$. Consequently, at the targets' frame reference time needed to move distances including the distance between

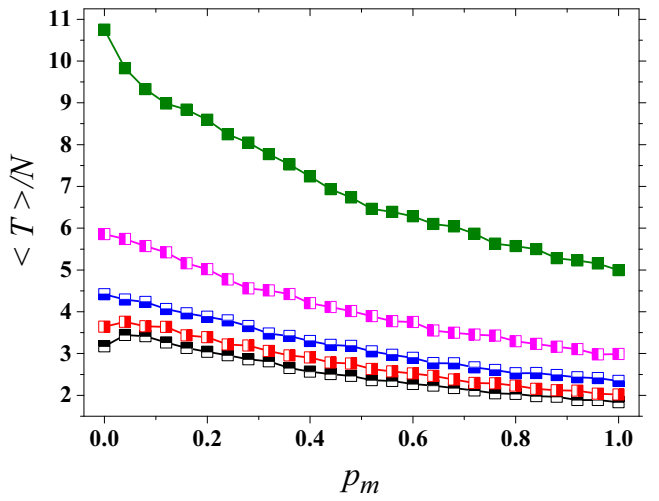

FIG. 20. $\langle T\rangle/N$ per p_m with $R = 30$ for $p = 0, 0.1, 0.2, 0.3$, and 0.4 from top to bottom. Based on analytical conclusion, we expect it to behave like $\langle T\rangle/N \sim (1 + p_m)$.

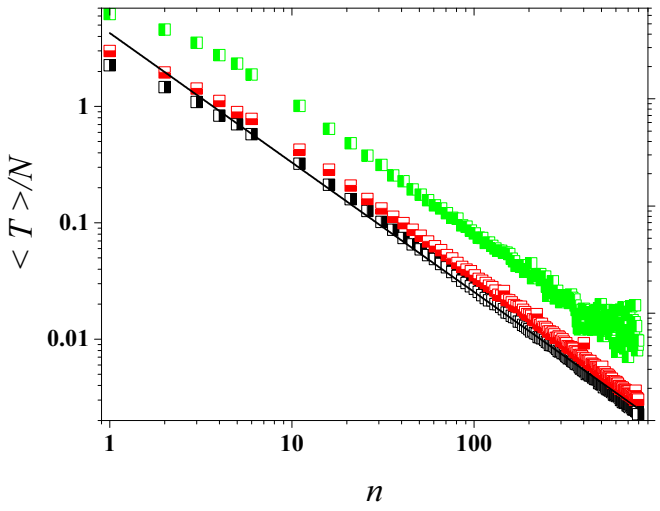

FIG. 21. Variation of $\langle T\rangle/N$ per number of targets n for $p = 0.4$, 0.2, and 0.0 from top to bottom. $\langle T\rangle D_{\text{eff}}/N$ fits $n^{-\kappa}$ with $\kappa = 1.11 \pm 0.05$.

the walker and target should be divided by $1 + p_m$. Figure 20 confirms this idea for all values of p.

The number of randomly distributed targets within medium changes the search time. We can estimate this relation analytically. Consider R_{exp} as the radius around initial position of the searching walker in which we expect it to see a target. When the searching walker is at the center of medium with N visitable sites, we can argue $R_{\text{exp}} \sim \sqrt{N}$ which for larger numbers of targets n, we have $R^2_{\text{exp}} \sim \langle T\rangle \sim \frac{N}{n}$ (Fig. 21).

12. Application to T cell migration analysis

By $\delta = 10$ μm and $\tau = 1$ min, dynamics of walker would be analogous to reports for T cells with speed of 10 μm min^{-1} [8,58]. Our model provides an alternative explanation for experimentally observed speed fluctuations of T cells [7,8] which is currently attributed to the morphology of lymph nodes [7,16]. Based on our result, speed fluctuations are an intrinsic feature of random motion; environmental features, including morphology of lymph nodes, might be able to alter the speed distribution but they can not be regarded as the source of fluctuations (see Figs. 7–9). Our study provides an explanation for seemingly contradictory reports where T cell migration was seen to be diffusive [9], subdiffusive [10], and superdiffusive [11]. Our model predicts that an inherently superdiffusive motion may effectively appear as diffusive or subdiffusive depending on the physical structure of the environment. T cell migration dynamics is thus defined by both internal and external determinants. Our model indicates that interpretation of measured migration dynamics has to be done with care; seemingly random motion of T cells in lymph nodes [9,62,63] cannot be interpreted as a uninform migration before deciphering the environmental effects on migration dynamics. Our model predicts that an intermediate value for chemoattractants gradient maximizes the efficiency of T cell search. We know that recently activated T cells can search for or follow cognate APCs [7,64] through chemotaxis and can move more than 500 μm under effect of chemoattractants [58,59]. Since the directionality of motion for immune cells is a function of chemoattractants' secretion rate and density [58], the efficiency of T cells search would be a function of chemoattractants gradient. As a result, in a crowded medium of tissue, an intermediate value of chemoattractants' gradient minimizes the search time. This prediction is readily testable experimentally. Recall that our results are valid for $R > \delta$, including $R = 30$, $\delta = 300$ μm. A T cell interacts typically with more than one target cell (e.g., APCs) during the immune response; however, it is not clear how target frequencies affect T cell search efficiency [7]. Our model predicts that for randomly moving T cells, the search time decreases as with the factor of n in which n is the number of targets and this relation holds almost for all densities below critical value. APCs are able to move and their migration is important in the immune response [65,66], but the implications of APC migration for T cell search efficiency has not been studied yet [7]. Our result predicts that motility of targets decreases the search time for all density of obstacles by the factor of $1 + D_{\text{APC}}/D$ in which D is the T cell diffusion constant and D_{APC} is the APC diffusion constant. APCs sometimes search for T cells [67], but it is not clear how that affects T cell search efficiency [7]. Here, our model predicts an intermediate value of chemoattractant gradient which minimizes the search time.

[1] A. M. Hein, F. Carrara, D. R. Brumley, R. Stocker, and S. A. Levin, Proc. Natl. Acad. Sci. USA **113**, 9413 (2016).
[2] D. H. Gire, V. Kapoor, A. Arrighi-Allisan, A. Seminara, and V. N. Murthy, Curr. Biol. **26**, 1261 (2016).
[3] Q. Gaudry, K. I. Nagel, and R. I. Wilson, Curr. Opin. Neurobiol. **22**, 216 (2012).
[4] A. Levchenko and P. A. Iglesias, Biophys. J. **82**, 50 (2002).
[5] R. Stocker, Science **338**, 628 (2012).
[6] A. Berdahl, C. J. Torney, C. C. Ioannou, J. J. Faria, and I. D. Couzin, Science **339**, 574 (2013).
[7] M. F. Krummel, F. Bartumeus, and A. Gérard, Nat. Rev. Immunol. **16**, 193 (2016).
[8] M. J. Miller, S. H. Wei, I. Parker, and M. D. Cahalan, Science **296**, 1869 (2002).
[9] M. J. Miller, S. H. Wei, M. D. Cahalan, and I. Parker, Proc. Natl. Acad. Sci. USA **100**, 2604 (2003).
[10] T. Worbs, T. R. Mempel, J. Bölter, U. H. von Andrian, and R. Förster, J. Exp. Med. **204**, 489 (2007).
[11] T. H. Harris, E. J. Banigan, D. A. Christian, C. Konradt, E. D. T. Wojno, K. Norose, E. H. Wilson, B. John, W. Weninger, A. D. Luster, A. J. Liu, and C. A. Hunter, Nature **486**, 545 (2012).
[12] G. M. Fricke, K. A. Letendre, M. E. Moses, and J. L. Cannon, PLoS Comput. Biol. **12**, e1004818 (2016).
[13] X. Zhou, R. Zhao, K. Schwarz, M. Mangeat, E. C. Schwarz, M. Hamed, I. Bogeski, V. Helms, H. Rieger, and B. Qu, Sci Rep. **7**, 44357 (2017).

[14] T. Lämmermann, B. L. Bader, S. J. Monkley, T. Worbs, R. Wedlich-Söldner, K. Hirsch, M. Keller, R. Förster, D. R. Critchley, R. Fässler *et al.*, Nature (London) **453**, 51 (2008).

[15] R. J. Petrie, A. D. Doyle, and K. M. Yamada, Nat. Rev. Mol. Cell Biol. **10**, 538 (2009).

[16] J. B. Beltman, A. F. Marée, J. N. Lynch, M. J. Miller, and R. J. de Boer, J. Exp. Med. **204**, 771 (2007).

[17] A. Wood, J. Cell Sci. **90**, 667 (1988).

[18] A. Webb, P. Clark, J. Skepper, A. Compston, and A. Wood, J. Cell Sci. **108**, 2747 (1995).

[19] N. Gomez, S. Chen, and C. E. Schmidt, J. R. Soc. Interface **4**, 223 (2007).

[20] A. I. Teixeira, G. A. Abrams, P. J. Bertics, C. J. Murphy, and P. F. Nealey, J. Cell Sci. **116**, 1881 (2003).

[21] W. Loesberg, J. Te Riet, F. van Delft, P. Schön, C. Figdor, S. Speller, J. van Loon, X. Walboomers, and J. Jansen, Biomaterials **28**, 3944 (2007).

[22] H. Salmon, K. Franciszkiewicz, D. Damotte, M.-C. Dieu-Nosjean, P. Validire, A. Trautmann, F. Mami-Chouaib, and E. Donnadieu, J. Clin. Invest. **122**, 899 (2012).

[23] R. Metzler and J. Klafter, Phys. Rep. **339**, 1 (2000).

[24] D. V. Nicolau, J. F. Hancock, and K. Burrage, Biophys. J. **92**, 1975 (2007).

[25] S. Coscoy, E. Huguet, and F. Amblard, Bull. Math. Biol. **69**, 2467 (2007).

[26] Y. Gefen, A. Aharony, and S. Alexander, Phys. Rev. Lett. **50**, 77 (1983).

[27] R. Rammal and G. Toulouse, J. Phys. Lett. **44**, 13 (1983).

[28] R. Rammal, J. Stat. Phys. **36**, 547 (1984).

[29] H. Böttger and V. Bryksin, Phys. Status Solidi B **113**, 9 (1982).

[30] M. Barma and D. Dhar, J. Phys. C: Solid State Phys. **16**, 1451 (1983).

[31] D. Dhar, J. Phys. A: Math. Gen. **17**, L257 (1984).

[32] D. Dhar and D. Stauffer, Int. J. Mod. Phys. C **9**, 349 (1998).

[33] A. Fribergh and A. Hammond, Commun. Pure Appl. Math. **67**, 173 (2014).

[34] A. Sapozhnikov *et al.*, Ann. Probab. **45**, 1842 (2017).

[35] A. Fribergh *et al.*, Ann. Probab. **38**, 1717 (2010).

[36] N. Berger, N. Gantert, and Y. Peres, Probab. Theory Relat. Fields **126**, 221 (2003).

[37] E. Daryaei and S. Rouhani, Phys. Rev. E **89**, 062101 (2014).

[38] K. Miller, ALEA, Lat. Am. J. Probab. Math. Stat **13**, 53 (2016) [Erratum: *ibid.* **14**, 173 (2017)].

[39] S. Havlin and D. Ben-Avraham, Adv. Phys. **36**, 695 (1987).

[40] M. T. Barlow *et al.*, Ann. Probab. **32**, 3024 (2004).

[41] S. Redner, *A Guide to First-passage Processes* (Cambridge University Press, Cambridge, 2001).

[42] O. Bénichou, M. Coppey, M. Moreau, P. H. Suet, and R. Voituriez, Phys. Rev. Lett. **94**, 198101 (2005).

[43] O. Bénichou, C. Loverdo, M. Moreau, and R. Voituriez, Rev. Mod. Phys. **83**, 81 (2011).

[44] M. Sheinman, O. Bénichou, Y. Kafri, and R. Voituriez, Rep. Prog. Phys. **75**, 026601 (2012).

[45] S. Condamin, O. Bénichou, and M. Moreau, Phys. Rev. Lett. **95**, 260601 (2005).

[46] S. Condamin, O. Bénichou, V. Tejedor, R. Voituriez, and J. Klafter, Nature (London) **450**, 77 (2007).

[47] O. Bénichou, C. Chevalier, J. Klafter, B. Meyer, and R. Voituriez, Nat. Chem. **2**, 472 (2010).

[48] O. Bénichou and R. Voituriez, Phys. Rep. **539**, 225 (2014).

[49] T. Guérin, N. Levernier, O. Bénichou, and R. Voituriez, Nature (London) **534**, 356 (2016).

[50] E. A. Codling, M. J. Plank, and S. Benhamou, J. R. Soc. Interface **5**, 813 (2008).

[51] A. A. Saberi, Phys. Rep. **578**, 1 (2015).

[52] O. Benichou, T. Guérin, and R. Voituriez, J. Phys. A: Math. Theor. **48**, 163001 (2015).

[53] E. F. Keller and L. A. Segel, J. Theor. Biol. **30**, 225 (1971).

[54] J. Textor, A. Peixoto, S. E. Henrickson, M. Sinn, U. H. von Andrian, and J. Westermann, Proc. Natl. Acad. Sci. USA **108**, 12401 (2011).

[55] E. J. Banigan, T. H. Harris, D. A. Christian, C. A. Hunter, and A. J. Liu, PLoS Comput. Biol. **11**, e1004058 (2015).

[56] R. Holland, J. Zool. **293**, 1 (2014).

[57] K. W. Tosney, Dev. Dyn. **229**, 99 (2004).

[58] Y. Wang and D. J. Irvine, Integr. Biol. **5**, 481 (2013).

[59] R. Minet-Quinard, M. C. Farges, E. Thivat, C. Deleine, G. Mayot, J. Brtko, J. Ribalta, B. Winklhofer-Roob, E. Rock, and M. P. Vasson, Immun. Ageing **7**, 10 (2010).

[60] Y. Wang and D. J. Irvine, Biomaterials **32**, 4903 (2011).

[61] E. Limpert, W. A. Stahel, and M. Abbt, BioScience **51**, 341 (2001).

[62] C. Beauchemin, N. M. Dixit, and A. S. Perelson, J. Immunol. **178**, 5505 (2007).

[63] M. D. Cahalan and I. Parker, Annu. Rev. Immunol. **26**, 585 (2008).

[64] F. Castellino, A. Y. Huang, G. Altan-Bonnet, S. Stoll, C. Scheinecker, and R. N. Germain, Nature (London) **440**, 890 (2006).

[65] G. J. Randolph, V. Angeli, and M. A. Swartz, Nat. Rev. Immunol. **5**, 617 (2005).

[66] T. Worbs, S. I. Hammerschmidt, and R. Förster, Nat. Rev. Immunol. **17**, 30 (2017).

[67] T. Okada, M. J. Miller, I. Parker, M. F. Krummel, M. Neighbors, S. B. Hartley, A. O'Garra, M. D. Cahalan, and J. G. Cyster, PLoS Biol. **3**, e150 (2005).